Surface enhanced infrared spectroscopy using metal oxide plasmonic antenna arrays.

Martina Abb,[†,§] Yudong Wang,[‡,§] Nikitas Papasimakis,[¶] C. H. de Groot,[‡] and Otto L. Muskens[*,†]

Physics and Astronomy, Faculty of Physical Sciences and Engineering, University of Southampton, Highfield, Southampton SO17 1BJ, United Kingdom, Nano group, Faculty of Physical Sciences and Engineering, University of Southampton, Highfield, Southampton SO17 1BJ, United Kingdom, and Optoelectronics Research Centre & Centre for photonic Metamaterials, University of Southampton, United Kingdom

E-mail: O.Muskens@soton.ac.uk

Abstract

We successfully demonstrate surface enhanced infrared spectroscopy (SEIRS) using arrays of indium-tin oxide (ITO) plasmonic nanoantennas. The ITO antennas show a strongly reduced plasmon wavelength, which holds promise for ultracompact antenna arrays and extremely subwavelength metamaterials. The strong plasmon confinement and reduced antenna cross section allows ITO antennas to be integrated at extremely high densities with no loss in performance due to long-range transverse interactions.

---

*To whom correspondence should be addressed

†Physics and Astronomy, Faculty of Physical Sciences and Engineering, University of Southampton, Highfield, Southampton SO17 1BJ, United Kingdom

‡Nano group, Faculty of Physical Sciences and Engineering, University of Southampton, Highfield, Southampton SO17 1BJ, United Kingdom

¶Optoelectronics Research Centre & Centre for photonic Metamaterials, University of Southampton, United Kingdom

§Contributed equally to this work

By further reducing the spacing of antennas in the arrays we access the regime of plasmonic near field coupling where the response is enhanced for both Au and ITO devices. Ultracompact ITO antennas with high spatial and spectral selectivity in spectroscopic applications offer a viable new platform for infrared plasmonics, which may be combined with other functionalities of these versatile materials in devices.

Keywords: nanoantenna; oxide plasmonics; conductive oxides; surface-enhanced infrared spectroscopy (SEIRS); surface-enhanced infrared absorption (SEIRA)

The large free carrier density and relatively small ohmic losses of the noble metals Au and Ag have enabled many of the breakthroughs in field enhanced spectroscopy.[1,2] With the maturation of plasmonics research and its growing relevance for technology, new combinations of plasmonic materials with complementary functionalities are being sought, which could improve performance or which could lead to entirely new application areas. Added values beyond Au and Ag include electrical, magnetic or chemical activity, low cost, and compatibility with industrial standards and processes (e.g. complementary metal-oxide-semiconductor CMOS). In addition, novel applications such as metamaterials and transformation optics have emerged which demand a greater flexibility in optical parameters.[3]

Alternative materials for plasmonics include a wide range of metals,[4] doped semiconductors,[5] metal oxides, nitrides,[6,7] and graphene-like two-dimensional materials.[8] Next to conventional applications in the visible and near-infrared spectral range, some of these materials target the mid infrared and terahertz domains, with applications in e.g. chemical sensing and security. The performance of various materials has been critically evaluated in a number of theoretical and experimental studies.[3,6,7]

Metal oxides are technologically highly important materials with many applications including oxide electronics,[9,10] solar cells,[11] chemical sensors[12,13] and catalysis.[13,14] Transparent conducting oxides (TCOs) are large bandgap dielectrics with a density of free carriers in between that of doped semiconductors and noble metals. Despite investigations of the plas-

2

monic response of metal oxides,[7,15–20] their performance in plasmon enhanced spectroscopy is yet unknown. Here we show that arrays of indium-tin oxide (ITO) plasmonic nanoantennas are highly suitable for surface enhanced infrared spectroscopy (SEIRS). SEIRS is a spectroscopic technique used to identify molecular fingerprints by resonant detection of infrared vibrational modes through coupling with the plasmonic modes of an antenna.[1,21–29] Most SEIRS studies so far have used the noble metals Au and Ag as these have been shown to produce strong SEIRS signatures with monolayer sensitivity. The combination of label-free infrared spectroscopy with the versatility of doped metal oxides has the potential of opening up new applications in sensing and spectroscopy, for example as multifunctional transparent electrodes, catalysts, or electrically or optically controllable plasmonic devices.[30,31] As we show here, oxide plasmonics provides a promising new platform for SEIRS with complementarity to and some advantages over their noble metal counterparts.

The optical response of TCOs can be described well using the Drude model for free electrons and is characterized by a dielectric behavior in the visible with a transition to metallic behavior in the infrared.[15,32] The density of free electrons can be controlled by adding electron donor dopants, and depends on material processing conditions.[7,11,15,20] TCOs can be achieved with electron densities exceeding 10^{21} cm^{-3}, resulting in a bulk plasmon wavelength in the near-infrared. A wide range of fabrication methods of TCOs include sputtering, evaporation, atomic layer deposition, and pulsed laser deposition.[11] To combine TCOs with standard nanofabrication techniques such as e-beam lithography and lift-off, we use here a combination of ITO evaporation at low temperatures, followed by post-annealing to increase the electron concentration similar to Ref.[20] We designed ITO nanorod antenna structures with equal height and width of 80 nm, and with a length varying between 0.15 μm and 4.5 μm. Arrays of Au antennas with exactly the same design parameters were fabricated in order to directly compare the plasmonic performance of both materials under identical conditions.

Antenna arrays were fabricated by e-beam lithography (JEOL 9300FS) on calcium fluo-

ride (CaF$_2$) substrates using a bilayer of copolymer (MMA 8.5 A from MicroChem, approx. 250 nm thickness) and polymethylmethacrylate (PMMA 495 A4 from MicroChem, approx. 150 nm thickness), with an additional 20 nm layer of conducting polymer (Espacer 300Z) to prevent charge up. After evaporation of 80 nm of ITO (ITO grains, $90 - 10$ $wt\%$, 99.99 pure from Testbourne Ltd.) from a ceramic crucible at 2×10^{-4} mbar partial oxygen pressure and subsequent lift-off, samples were annealed at 200°C for one hour. Antenna arrays of 120 μm $\times$ 120 μm were fabricated for infrared spectroscopy. The height of the antennas was characterized using a contact profilometer and were found to be 80 ± 5 nm for both the ITO and Au arrays. Electrical Hall measurements showed a carrier concentration of around $1.5 \pm 0.5 \times 10^{21}$ cm^{-3}, a mobility of 13.6 cm^2/Vs and a sheet resistance of 39.4 Ohms/square. Drude model fits to the optical reflectivity spectra of the ITO layer resulted in a bulk plasmon wavelength λ_p of 685 nm, and $\epsilon_\infty = 3.8$, indicating a free electron density of 1.25×10^{21} cm^{-3}. The value for the plasmon frequency was considered more accurate than the Hall measurement and was used in further analysis.

Infrared spectra were measured in transmission using a Jasco FTIR-4200 with a liquid-nitrogen-cooled mercury cadmium telluride detector, with the polarization set along the long axis of the nanoantennas. Each measurement was averaged over 100 scans and the CaF$_2$ substrate was used as a reference. The references and the array spectra were collected with a resolution of 16 cm^{-1}. For the SEIRS experiment, an approx. 50 nm thin layer of PMMA 495 A2 was spincoated onto the ITO and gold antenna substrates at 5000 rpm for 45 s and then baked at 180 degrees for 70 s. FTIR measurements were taken directly after the thin PMMA film was deposited.

Figure 1a shows scanning electron microscopy (SEM) images arrays of ITO antennas fabricated using e-beam lithography on a CaF$_2$ substrate (see Supporting Information Figure S1 for additional SEM images). The antenna arrays consist of nanorods of length L, which are separated both horizontally and vertically by a spacing s. Arrays with spacings of 600 nm and 300 nm were fabricated. In addition, we investigate arrays of dimer nanoantennas with an

4

antenna gap of 50 nm and a spacing of 300 nm. The SEM images reveal high reproducibility of the ITO antennas with dimensions closely matching the design parameters.

Figures 1b and c show the transmission spectra of arrays with different nanorod lengths L both for Au (b) and ITO (c). The broad dips in the transmission spectra correspond to longitudinal surface plasmon resonances of the nanorods. These resonances shift to lower energy with increasing antenna length. Compared to the Au antennas, the ITO antennas show infrared resonances for much shorter antenna lengths. Additionally, the transmission dips are less strong for the ITO than for Au, indicating a reduced extinction per antenna. Comparing arrays with the same density of antennas, we find that the resonance length is around three to four times smaller for the ITO than for the Au arrays. Compared to the bare antenna arrays (see Supporting Information Figure S2), the PMMA-coated arrays show a number of narrow vibrational resonances in the spectra indicative of SEIRS, which will be discussed further below.

The reduction of the resonant antenna length for ITO is related to its dielectric function $\epsilon = \epsilon_1 + i\epsilon_2$. Figure 2a shows the calculated dielectric function (black lines) using the free carrier density of 1.25×10^{21} cm^{-3}. Whereas the dielectric function of Au in the infrared (red lines) approaches that of a perfectly conductor ($\epsilon_1 = -\infty$), the ITO response is characterized by a much lower real part of ϵ. Unlike perfect conductors, metals and semiconductors in the visible and IR spectrum do not follow a simple direct correlation between antenna length and resonance wavelength of light, but instead an effective wavelength scaling needs to be employed in order to take into account the finite skin depth. Figure 2b shows the experimental resonance positions for the $s = 600$ nm and $s = 300$ nm arrays against nanorod length. The effective wavelength scaling for the Au antennas (red line) was obtained using the analytical relation for the TM$_0$ modes of a cylindrical waveguide.[33] A similar scaling relation was obtained by using the Drude model parameters for ITO without any free parameters (black line). In both cases, an effective dielectric function was taken as the geometrical average of the substrate and air, including the wavelength dependent refractive index of the

CaF$_2$ substrate through a Sellmeyer equation.

Our experimental data agrees well with this scaling, which predicts a factor of three increase in the surface plasmon wavelength of ITO nanorods compared to Au rods of the same length. This property means that ITO antennas can be made more compact and allows achieving an even greater packing density. In previous experiments on individual Au nanoantennas,[26] a resonance frequency of 9.3 μm was reported for a $L = 3.4$ μm antenna. Compared to single antennas, the Au arrays of this study show a significant blue shift, which can be attributed to the transverse coupling of antennas in the array.[34] Transverse coupling strongly limits the integration density that can be achieved for Au antennas.[22,25,26,34,35]

Compared to Au, the spectral resonance positions for ITO antenna arrays in Figure 2b do not depend on antenna spacing. This suggests that the ITO antennas are much less affected by interparticle coupling. This observation is supported by results shown in Figure 2c and d. A number of different figures of merit have been defined to compare the performance of different plasmonic materials.[3,6] Here, we investigate the resonance quality factor Q_{tot}, which characterizes the decay of the plasmon mode due to nonradiative and radiative damping. Similar to previous nanoparticle linewidth studies,[36] we use the half-maximum width at the low frequency side of the resonances, which is not affected by higher order modes, to determine the quality factor. Figure 2c and d show results for the different arrays under study.

We compare our experimental results with the nonradiative and radiative contributions to Q_{tot} defined according to $Q_{\text{tot}} = \omega_{\text{res}}/\Gamma_{\text{tot}}$ with $\Gamma_{\text{tot}} = \Gamma_{\text{NR}} + \Gamma_R$ the total decay rate and ω_{res} the resonance angular frequency. For the nonradiative contribution we use the general expression for a dipole oscillator $\Gamma_{NR} = 2\epsilon_2/(\partial\epsilon_1/\partial\omega)$.[37,38] This expression is to good approximation equal to the Drude damping rate γ_D in absence of interband absorption and under the condition $\omega > \gamma_D$. The nonradiative quality factor for Au (dashed line in Fig. 2c) peaks at a value of $Q_{\text{NR}} \simeq 22$ in the near infrared, in agreement with measurements for small Au nanorods.[37,39] In the infrared, Q_{NR} drops significantly for both materials as the

optical frequency is reduced, while the damping rate stays constant. Thus the number of optical cycles stored in the resonator goes down, and the antennas become critically damped for $Q_{NR} < 1$.

The radiative decay was calculated using a microscopic theory for the radiation response of individual electrons in the antenna,[40] resulting in the expression $\Gamma_R = \omega^2 n_e^2 V^2 e^2 / 6\pi\epsilon_0 c^3$, with n_e the electron density, V the nanoantenna volume and c the speed of light. The high electron density of Au results in a strong radiation damping (dash-dotted line in Fig. 2c), which contributes significantly to Q_{tot}. In comparison, the much lower electron density of ITO compared to Au, combined with the shorter resonance length of the antenna, results in a strong suppression of the radiation damping, and thus a high Q_R (dash-dotted line in Fig. 2d). The total quality factor for the ITO antennas is governed entirely by the nonradiative component Q_{NR} (solid line in Fig. 2d). From the direct relation between radiated power and polarizability,[40] the smaller radiated power means that antenna coupling through far-field (dipole-dipole) interaction is significantly reduced, and antennas can be spaced closer without suppression of the resonance quality. This result from the analytical expression is confirmed by numerical simulations as will be shown further below.

Next, we investigated the performance of ITO antenna arrays in one of the most prominent applications of plasmonics in the mid infrared, Surface Enhanced Infrared Spectroscopy (SEIRS). Infrared absorption and its enhancement by metallic surfaces has been known since the early days of surface enhanced spectroscopy.[1] Au antennas have been shown to produce a strong SEIRS response.[21–29] For the SEIRS experiments, we used a thin, 50-nm layer of PMMA which was spincoated onto the antenna arrays. The presence of the PMMA can be observed in Fig. 1 as a number of sharp resonances on top of the extinction spectrum of the antennas. The vibrational spectra were separated from the broad antenna resonance by subtracting a 50-point moving average from each curve (see Supporting Information Figure S3). Resulting SEIRS spectra are shown in Fig. 3 for the arrays of dimer antennas with different lengths L, while spectra for the other arrays are shown in Supporting Information Figure

S4. Vibrational modes of the PMMA can be identified corresponding to C-O-C (1140 cm^{-1}), C-O (1250 cm^{-1}), C-H (1450 cm^{-1}) and C=O (1720 cm^{-1}) stretching modes.

Both the Au and ITO antennas show a strongly resonant behavior of the SEIRS intensity with antenna length. The SEIRS amplitude is weak both for very short and very long antennas, and shows a strong enhancement for intermediate antenna lengths around 1 μm. We analyzed the 'fingerprint contrast' ΔC,[26] defined as the dip-to-peak transmission change between the lowest and highest transmission for a vibrational mode as indicated for a typical mode in Figure 3. Similar to the SEIRS transmission spectra, ΔC has the unit of % transmission. Results are shown in Fig. 4a,b for the strongest vibrational mode around 1720 cm^{-1} and for the three different types of Au (a) and ITO (b) arrays under study. As predicted by previous theoretical studies,[26] the SEIRS response shows a shift of the resonance condition compared to the far-field extinction measured at the same frequency (black diamonds). This typical behavior could also be observed in the spectra of Fig. 1 and is a clear demonstration of the fact that the SEIRS enhancement is proportional to the near-field resonance of the antenna. The near-field resonance is redshifted compared to the far-field extinction,[26,41,42] and thus the SEIRS resonance occurs for shorter antennas both for the cases of Au and ITO.

The effect of array density on the SEIRS response confirms our interpretation of the far-field extinction, namely, that the long-range transverse coupling strongly affects the response of the Au antenna array. The maximum SEIRS signal for Au is reduced for the $s = 300$ nm compared to the $s = 600$ nm arrays, even though the antenna density is increased. In comparison, the signal strength for ITO is increased by a factor two upon reducing the spacing, in agreement with the increase in area fraction (see Supporting Information Figure S5). High density integration of ITO antennas thus improves the overall response. The SEIRS response for the Au antennas is partially recovered by pairing the rods into dimer antennas, which is attributed to the larger field enhancement associated with the plasmonic hot spot in the antenna gap. We note that the obtained values are of the same order as the 8% contrast predicted for PMMA using a single Au nanorod antenna of similar dimensions.[26]

The experimental SEIRS results for the ITO antennas are compared to numerical calculations of the plasmonic near field enhancement of individual ITO antennas obtained using the boundary element method.[43] Figure 5a shows the near-field maps of single and dimer nanorod antennas, while in Figure 5b,c we present the dependence of the near field intensity and the far field extinction $1 - T$ at 1720 cm^{-1} on antenna length. Excellent agreement is found between the calculated near field intensities of Figure 5b,c and the experimental SEIRS results of Fig. 4c. The simulations confirm the resonant enhancement of the near field at an energy of 1720 cm^{-1} for antenna lengths around 0.75 μm. For the calculated single rod, the near field intensity at 25 nm away from the antenna reaches values up to 125, with maximum E^2 values at the antenna surface reaching up to around 400 (cf. Fig. 5a). In comparison, Au nanorods show intensity enhancements of up to 2000,[21,22] however such values generally cannot be achieved in high density arrays.[34,35]

To further assess the effect of antenna coupling in high density ITO and Au arrays for field enhanced spectroscopy, we calculated the near field response of a realistic antenna on substrate geometry using a finite element model (COMSOL). Single-particle scattering and absorption cross sections are shown in Figure 6a,b for isolated Au ($L = 1.5$ μm, a) and ITO ($L = 0.75$ μm, b) rods. While the absorption cross sections are similar for both rods, the scattering efficiency of the ITO is strongly reduced. The reduced scattering cross section of the ITO nanorod is in qualitative agreement with the analytical model for radiation damping (cf. Fig. 2d). Next, the antenna coupling was taken into account by adding periodic boundary conditions, where the size of the unit cell was varied according to the spacing parameter s. In order to estimate the integrated SEIRS response over the array, the square of the local electric field was averaged over a plane positioned 20 nm above the substrate. Figure 6c and d show the resulting enhancement, normalized to the incident intensity, for a range of parameters L and s. For the Au, we see two regimes of large enhancement, corresponding to far-field diffractive coupling at large s and near-field interaction for small s.[35] The near-field coupling is associated with a strong shift of the resonance to shorter antenna lengths

9

L. The calculation for Au antennas shows that reducing the spacing from $s = 600$ nm to $s = 300$ nm results in lower enhancement, as observed in experiments. The ITO antennas show a monotonous increase of the resonant intensity enhancement with reduced spacing. Only for spacings s below 300 nm a spectral shift is observed attributed to near-field coupling.

The numerical simulations predict that the SEIRS enhancement can be further enhanced for spacings less than 300 nm. In an attempt to achieve this regime of strong near-field interaction, we modified our e-beam fabrication to a 3-layer process, including a thin Si layer to limit the underetching of the PMMA resist.[45] Using this method, spacings as small as 100 nm could be obtained as shown by the SEM images in the inset of Fig. 6e,f. Additional SEM images and full analysis of spectra are presented in the Supporting Information Figure S6, S7, and S8. The resulting SEIRS fingerprint contrast for the new arrays is shown in Fig. 6e,f. The results confirm the trend of the simulations, namely that further reduction of the spacing results in an additional increase of the SEIRS enhancement and a shift of the resonance length. The new process resulted in increased antenna widths of around 120 nm for the case of Au, therefore the values of Fig. 6e,f cannot be directly compared with the data in Fig. 4. Better agreement was obtained for ITO, resulting in similar values for the $s = 300$ nm array between samples. We emphasize that this regime of extremely high density arrays has not been previously studied in SEIRS spectroscopy even for the case of Au. The possibility to (partially) overcome performance loss for Au arrays at high densities through near-field interactions may be of importance for applications benefiting from such high-density integration, e.g. for chemistry or sensing.

An important factor determining the potential of metal oxide antennas as new elements for infrared plasmonics is their stability. Supporting Information Figure S9 shows the plasmon resonance and SEIRS response of the $L = 0.5$ μm ITO dimer antenna after 15 weeks of storage in a nitrogen purged dessicator cabinet. No marked degradation in performance was observed, indicating a good shelf lifetime of the arrays under study. Stability in specific applications will depend on the chemical environment and experimental conditions (e.g.

humidity, temperature) and will require more detailed studies.[46]

In conclusion, we have demonstrated that high density arrays of ITO antennas are very suitable for applications in surface enhanced infrared spectroscopy. While the plasmonic field enhancement by an individual ITO antenna is less strong than that of an equivalent Au antenna, the ITO antennas are found to be less sensitive to long-range transverse coupling, which allows their integration into ultracompact nanoantenna arrays or extremely subwavelength metamaterials. The weak interactions for ITO antennas will provide an increased simplicity of design compared to the strong interactions between adjacent elements found for Au. Because of the resulting high integration density of plasmonic hotspots per unit of area, ITO antenna arrays can deliver similar performance in surface enhanced IR spectroscopy as their noble metal counterparts. Using spin-coated PMMA, the SEIRS enhancement was systematically studied over 162 different antenna arrays, yielding excellent reproducibility. For the first time, we have explored the regime of extremely high density antenna arrays which showed improved response by near-field interaction both for Au and ITO. The combination of label-free infrared spectroscopy with the versatility of doped metal oxides has the potential of opening up new directions in sensing and spectroscopy. Metal oxides are finding widespread use as transparent electrodes, advanced (e.g. heat-reflecting) coatings, and catalysts. The possibility, by nanostructuring, to design resonant antennas at high density will allow including a plasmon-enhanced spectroscopic functionality in these types of applications. A particularly exciting prospect is the possibility for oxide plasmonics to be integrated with oxide nanoelectronics in order to achieve active plasmonic, transistor-type devices for tunable infrared sensors and for electronic-photonic integrated circuits.

Acknowledgement

Supporting Information Available

Supporting Information with Scanning Electron Microscopy images of Au and ITO antennas, infrared spectra and SEIRS response for all nanorod antenna arrays, calculated area fraction against antenna length, ITO stability studies. This material is available free of charge via the Internet at http://pubs.acs.org. This material is available free of charge via the Internet at `http://pubs.acs.org/`.

The authors declare no competing financial interest.

References

(1) Moskovits, M. *Rev. Mod. Phys.* **1985**, 57, 783-826.

(2) Halas, N. J.; Lal, S.; Chang, W.-S.; Link, S.; Nordlander, P. *Chem. Rev.* **2011**, 111, 3913-3961.

(3) Tassin, P.; Koschny, T.; Kafesak, M.; Soukoulis, C. M. A *Nat. Photon.* **2012**, 6, 259-264.

(4) Knight, M. W.; Liu, L.; Wang, Y.; Brown, L.; Mukherjee, S.; King, N. S.; Everitt, H. O.; Nordlander, P.; Halas, N. J. *Nano Lett.* **2012**, 12, 6000-6004.

(5) Law, S; Yu, L; Rosenberg, A.; Wasserman, D. *Nano Lett.* **2013**, **13)**, 4569-4574.

(6) West, P. R.; Ishii, S.; Naik, G. V.; Emani, N. K.; Shalaev, V. M.; Boltasseva, A. *Laser Photon. Rev.* **2010**, 4, 795-808.

(7) Naik, G. V.; Shalaev, V. M.; Botasseva, A. *Adv. Mater.* **2013**, 25, 3264-3294.

(8) Chen, J.; Badioli, M.; Alonso-González, P.; Thongrattanasiri, S.; Huth, F.; Osmond, J.; Spasenović, M.; Centeno, A.; Pesquera, A.; Godignon, P.; Zurutuza Elorza, A.;

Camara, N.; García de Abajo, F. J.; Hillenbrand R.; Koppens, F. H. L. *Nature* **2012**, 487, 77-81.

(9) Waser, R.; Aono, M. *Nature Mater.* **2007**, 6, 833-840.

(10) Dattoli, E. N.; Wan, Q.; Guo, W.; Chen, Y.; Pan, X.; Lu, W. *Nano Lett.* **2007**, 7, 2463-2469.

(11) Granqvist, C. G. *Solar En. Mat. & Sol. Cells* **2007**, 91, 1529-1598.

(12) Comini, E.; Baratto, C.; Faglia, G.; Ferroni, M.; Vomiero, A.; Sberveglieri, G. *Progr. Mater. Sc.* **2009**, 54, 1-67.

(13) Kolmakov, A.; Moskovits, M. *Annu. Rev. Mater. Res.* **2004**, 34, 151-180.

(14) Zhang, X.; Chen, Y. L.; Liu, R.-S.; Tsai, D. P. *Rep. Prog. Phys.* **2013**, 76, 046401.

(15) Brewer S. H.; Franzen S., *J. Phys. Chem. B* **2002**, 106, 12986-12992.

(16) Rhodes, C.; Cerruti, M.; Efremenko, A.; Losego, M.; Aspnes, D. E.; Maria, J.-P.; Franzen, S. *J. Appl. Phys.* **2008**, 103, 093108.

(17) Noginov, M. A.; Gu, L.; Livenere, J.; Zhu, G.; Pradhan, A. K.; Mundle, R.; Bahoura, M.; Barnakov, Yu. A.; Podolskiy, V. A. *Appl. Phys. Lett.* **2011**, 99, 021101.

(18) Li, S. Q.; Guo, P.; Zhang, L.; Zhou, W.; Odom, T. W.; Seideman, T.; Ketterson, J. B.; Chang, R. P. H. *ACS Nano* **2011**, 5, 9161-9170.

(19) Caglayan, H.; Hong, S.-H.; Edwards, B.; Kagan, C. R.; Engheta, N. *Phys. Rev. Lett.* **2013**, 111, 073904.

(20) Kim, J.; Naik, G. V.; Emani, N. K.; Guler, U.; Boltasseva, A. *IEEE J. Sel. Top. Quant. Electron.* **2013**, 19, 4601907.

(21) Neubrech, F.; Pucci, A.; Walter, T. W.; Karim, S.; Garcia-Etxarri, A.; Aizpurua, J. *Phys Rev. Lett.* **2008**, 101, 157403.

(22) Adato, R.; Yanik, A. A.; Amsden, J. J.; Kaplan, D. L.; Omenetto, F. G.; Hong, M. K.; Erramilli, S. ; Altug, H. *Proc. Nat. Acad. Sc.* **2009**, 106, 19227-19232.

(23) Le, F.; Brandl, D. W.; Urzhumov, Y. A.; Wang, H.; Kundu, J.; Halas, N. J.; Aizpurua, J.; Nordlander, P. *ACS Nano* **2008**, *2*, 7070-718.

(24) Aksu, S.; Yanik, A. A.; Adato, R.; Artar, A.; Huang M.; Altug, H. *Nano Lett.* **2010**, 10, 2511-2518.

(25) Adato R.; Altug, H. *Nat. Comm.* **2012**, 4, 2154.

(26) Alonso-González, P.; Albella, P.; Neubrech, F.; Huck, C.; Chen, J.; Golmar, F.; Casanova, F.; Hueso, L. E.; Pucci, A.; Aizpurua, J.; Hillenbrand R., *Phys. Rev. Lett.* **2013**, 110, 203902.

(27) Dregely, D.; Neubrech, F.; Duan, H.; Vogelgesang R.; Giessen, H. *Nat. Comm.* **2013**, 4, 2237.

(28) D'Andrea, C.; Bochterle, J.; Toma, A.; Huck, C.; Neubrech, F.; Messina, E.; Fazio, B.; Marago, O. M.; Di Fabrizio, E.; Lamy de la Chapelle, M.; Gucciardi, P. G.; Pucci, A. *ACS Nano* **2013**, 7, 3522-3531.

(29) Brown, L. V.; Zhao, K.; King, N.; Sobhani, H.; Nordlander, P.; Halas, N. J., *J. Am. Chem. Soc.* **2013**, 135 (9), 36883695.

(30) Feigenbaum, E.; Diest, K.; Atwater, H. A. *Nano Lett.* **2010**, 10, 2111-2116.

(31) Abb, M.; Albella, P.; Aizpurua, J.; Muskens, O. L. *Nano Lett.* **2011**, 11, 2457-2463.

(32) Edwards, P. P.; Porch, A.; Jones, M. O.; Morgan D. V.; Perks R. M. *Dalton Trans.* **2004**, 2995-3002, DOI: 10.1039/ b408864f.

(33) Novotny, L. *Phys. Rev. Lett.* **2007**, 98, 266802.

(34) Weber, D.; Albella, P.; Alonso-Gonzalez, P.; Neubrech, F.; Gui, H.; Nagao, T.; Hillen-
brand, R.; Aizpurua, J.; Pucci, A. *Opt. Expr.* **2011**, 19, 15047-15061.

(35) Simpkins, B. S.; Long, J. P.; Glembocki, O. J.; Guo, J.; Caldwell, J. D.; Owrutsky, J.
C. *Opt. Expr.* **2012**, 20, 27725-27739.

(36) Berciaud, S.; Cognet, L.; Tamarat, P.; Lounis, B. *Nano Lett.* **2005**, 5, 515518.

(37) Hu, M.; Novo, C.; Funston, A.; Wang, H.; Staleva, H.; Zou, S.; Mulvaney, P.; Xia, Y.;
G. V. Hartland, *J. Mater. Chem.* **2008**, 18, 1949-1960.

(38) Stockman, M., *Opt. Expr.* **2011**,19, 22029-22106.

(39) Sönnichsen, C.; Franzl, T.; Wilk, T.; von Plessen, G.; Feldmann, J.; Wilson, O.; Mul-
vaney, P., Phys. Rev. Lett. **2002**, 88(7), 077402.

(40) Kats, M. A.; Yu, N.; Genevet P.; Gaburro, Z.; Capasso, F. *Opt. Expr.* **2011**, 19,
21748-21753.

(41) Zuloaga, J.; Nordlander, P., *Nano Lett.* **2011**, 11, 1280 - 1283.

(42) Moreno, F.; Albella, P.; Nieto-Vesperinas, M., *Langmuir* **2013**, 29, 6715-6721.

(43) Garcia de Abajo, F. J.; Howie, A. *Phys. Rev. Lett.* **1998**, 80, 5180-5183.

(44) Johnson, P. B.; Christy, R. W. *Phys. Rev. B* **1972**, 6, 4370.

(45) Etrillard, J.; Bellessa, J.; Izrael, A, *Microel. Eng.* **1987**, 7, 11-20.

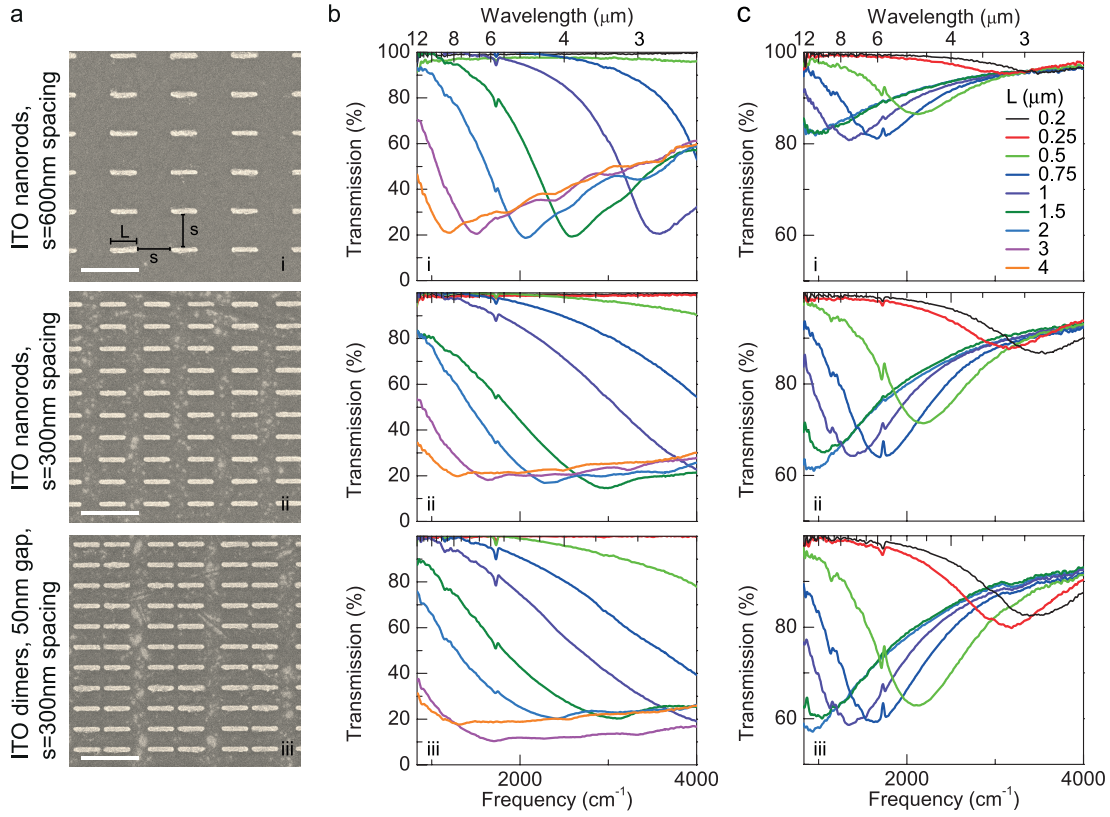(46) Romain, A.C., Nicolas, J., *Sens. Actuat.* **2010**, 146, 502-506.

Figure 1: a Scanning electron microscopy (SEM) images of ITO antenna arrays with $L = 0.5\ \mu$m for spacings $s = 600$ nm (i) and $s = 300$ nm (ii), and dimer antennas with 50 nm gap and $s = 300$ nm (iii). b,c Infrared transmission spectra of Au (b) and ITO (c) antenna arrays corresponding to typical array geometries presented in a and for various nanorod lengths L. The arrays were covered with a 50 nm PMMA layer, resulting in sharp SEIRS features due to plasmon coupling with vibrational resonances.

16
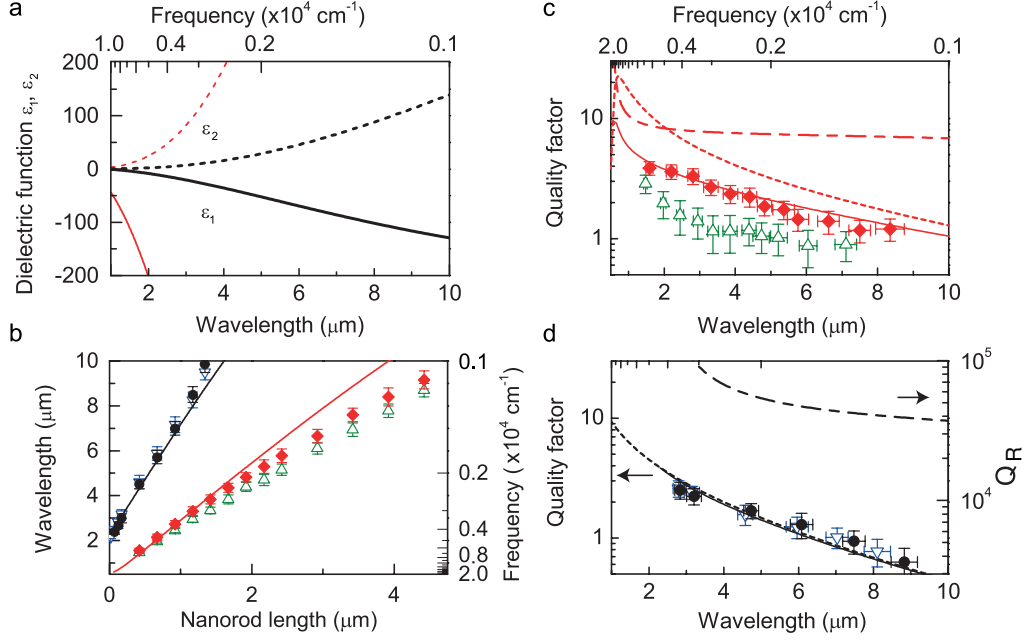
Figure 2: a Real (solid, ϵ_1) and imaginary (dashed, ϵ_2) parts of the dielectric functions of Au (red) and ITO (black) obtained using Drude model fits to experimental data from Johnson and Christy[44] and from reflectivity data for ITO ($n_e = 1.25 \times 10^{21} \mathrm{cm}^{-3}$). b Effective wavelength scaling of the antenna resonances for Au (red dots / green upward triangles) and ITO (black dots, blue downward triangles) antenna arrays with respectively $s = 600$ / $s = 300$ nm antenna separation. Lines are solutions of the resonance position of the TM_0 mode for a cylindrical waveguide using the theory of Novotny[33] using the dielectric functions of a. No free parameters were used in this model. c,d Quality factor of antenna resonance for Au (c) and ITO (d) antennas. Dashed lines: Q_{NR}, dash-dotted lines: Q_R, full lines: Q_{tot} (see Methods).
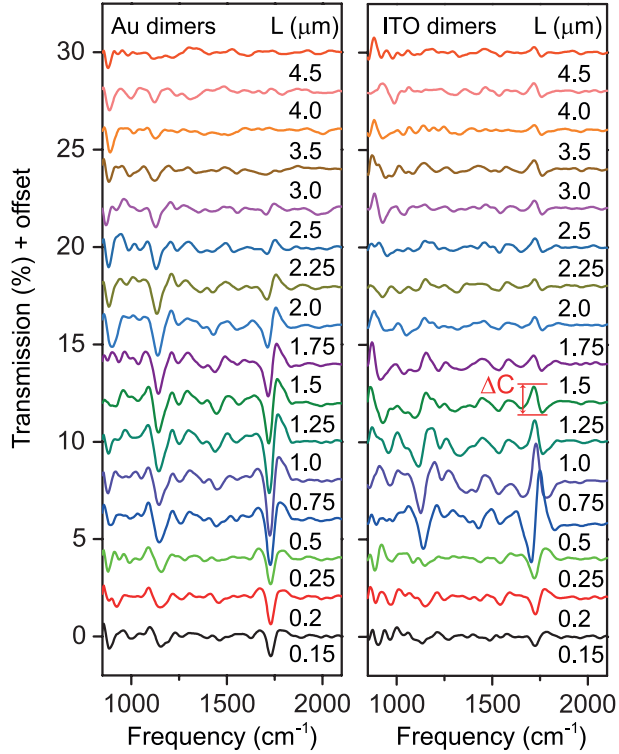
Figure 3: Vibrational spectra obtained using SEIRS, taken by subtracting 50-pt smoothed curve from spectra of Fig. 1b and c, for dimer antennas (iii). Results for nanorod arrays (i) and (ii) are shown in the Supporting Information Figure S4. Arrow shows definition of fingerprint contrast ΔC.
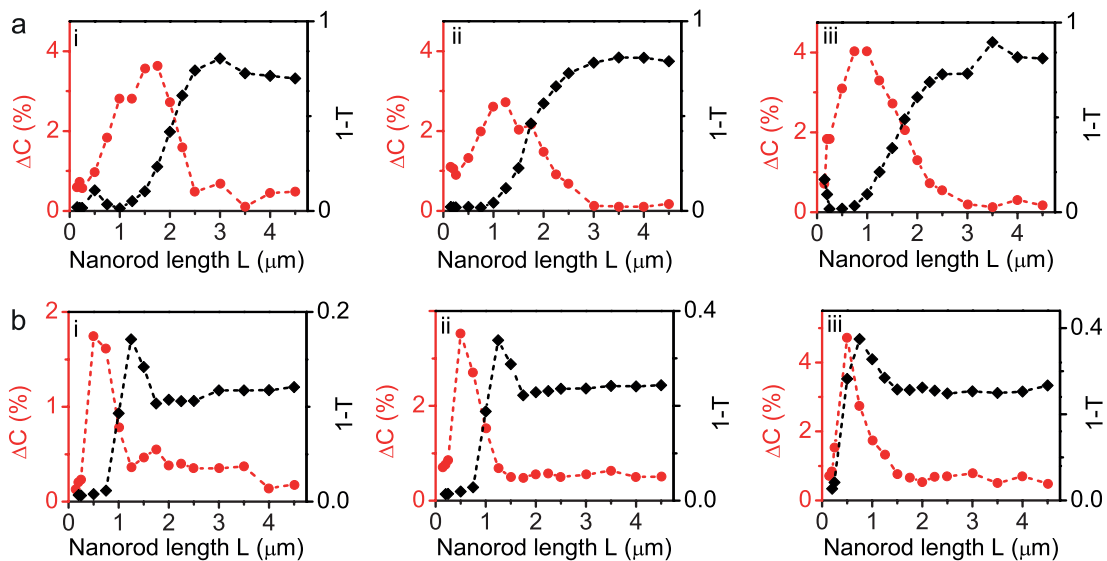

Figure 4: a,b 'Fingerprint contrast' ΔC obtained by taking peak to peak amplitude of mode at 1720 cm^{-1} (red dots), and extinction $1 - T$ at same frequency, for antenna arrays corresponding to (i)-(iii) of Fig. 1 for Au (a) and ITO (b).
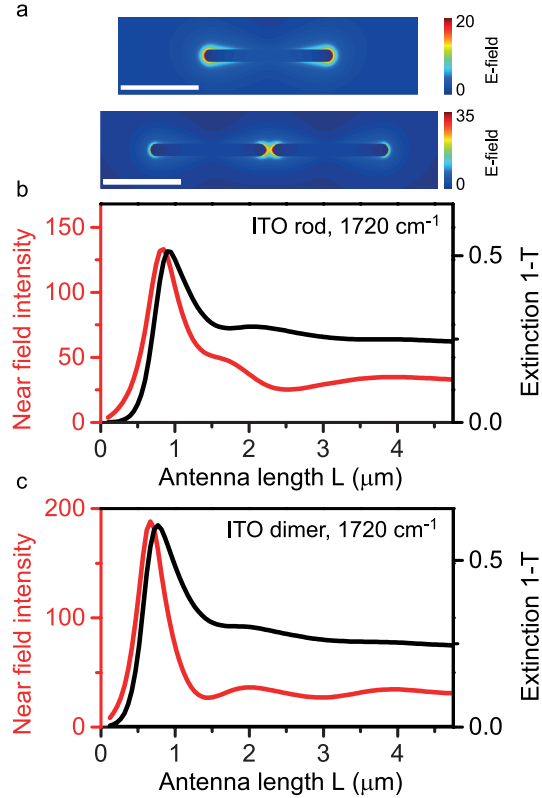
Figure 5: a Electric field maps of a $L = 0.83$ μm ITO nanorod antenna and a $L = 0.75$ μm ITO dimer antenna, corresponding to the maximum of the near field resonance at 1720 cm^{-1}. Scale bars, 0.5 μm. b Calculated near field intensity enhancement 25 nm from nanorod end cap(red, left axis) and far field extinction $1 - T$ (black, right axis) using single-particle cross-section, assuming spacing of $s = 300$ nm. c Same for array of dimer antennas with gap of 50 nm and $s = 300$ nm; near field intensity taken at the center of the antenna gap.
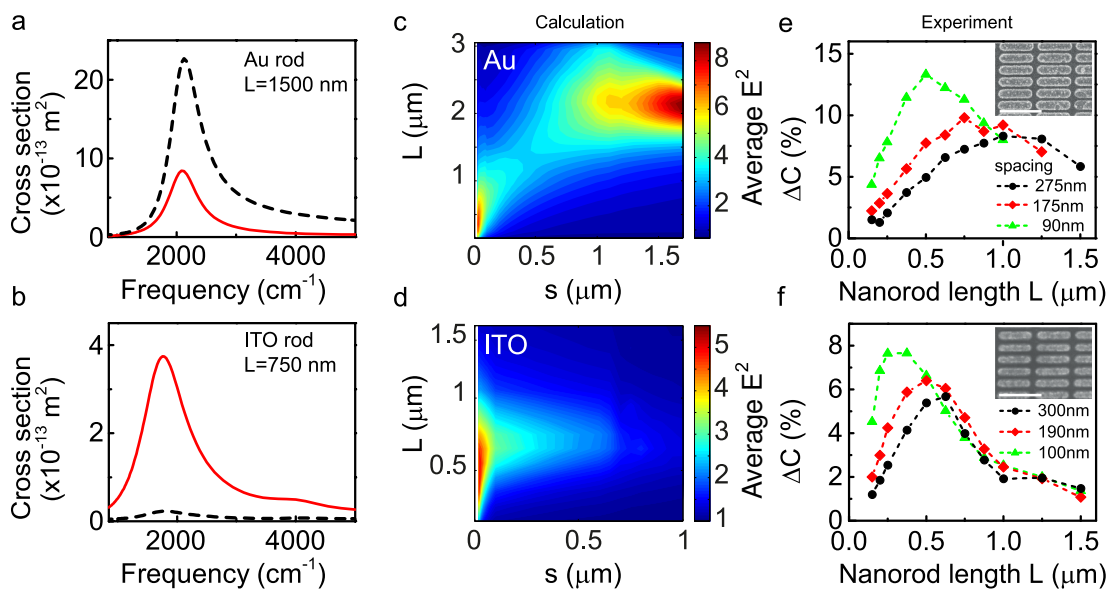
Figure 6: a, b Calculated far-field absorption (solid line, red) and scattering (dashed line, black) cross sections for isolated $L = 1500$ nm Au (a) and $L = 750$ nm ITO (b) rods on a CaF$_2$ substrate. c, d Maps showing the average intensity enhancement over a plane at 20 nm above the substrate, for periodic arrays with spacings s and antenna lengths L, for Au (c) and ITO (d). e, f Experimental fingerprint contrast for arrays with spacings between 90 nm and 300 nm (see legend), for Au and ITO. Insets: SEM images for arrays with smallest spacings, scale bar: 500 nm. Full analysis is shown in Supporting Information Figures S6-S8.